RSC Advances

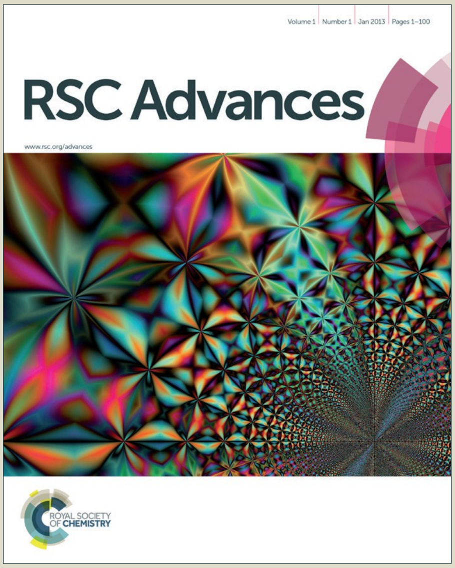

ROYAL SOCIETY
OF **CHEMISTRY**

www.rsc.org/advances

Journal Name

ARTICLE

Received 00th January 20xx,
Accepted 00th January 20xx

DOI: 10.1039/x0xx00000x

www.rsc.org/

Nanocomposites by the use of Simultaneous Twin Polymerization: tin alloys in a carbon / silica matrix

Christian Leonhardt,[a] Andreas Seifert,[b] Szilard Csihony,[c] Heino Sommer,[c] Michael Mehring*[a]

Twin Polymerization is a novel nonaqueous route to synthesize organic-inorganic hybrid materials composed of interpenetrating phase nanodomains. Here we present the Simultaneous Twin Polymerization (STP) of 2,2'-spirobi[4*H*-1,3,2-benzodioxasiline] (Si-spiro) in the presence of tin(II)-2,4-dimethoxyphenylmethanolate (**1**) mixed with a variety of metal additives, such as iron(III), nickel(II), copper(II) and cobalt(II) carboxylates. Nanocomposites composed of nanostructured tin alloys embedded in a carbon / silica matrix were obtained after treatment of the hybrid materials under reductive conditions using hydrogen. This approach allows the synthesis of a variety of tin alloys such as Sn_2Co, Sn_2Fe, Sn_2Ni_3, Sn_3Ni_4 and Sn_5Cu_6 which are embedded in a porous carbon/ silica matrix. The as-prepared nanocomposites show BET surface areas up to 327 m^2/g and particles sizes of the tin alloys in the range of a few to hundred nm. High-angle annular dark field scanning transmission electron microscopy (HAADF STEM) reveals a homogeneous distribution of the nanoparticular tin alloys in the carbon / silica matrix, which makes the nanocomposites to be potential anode materials for lithium-ion batteries as was demonstrated for the Sn_2Ni_3-based material.

Introduction

There is an ongoing interest in the development of novel synthetic strategies for nanostructured hybrid materials, that allow the modulation of structure, phase domain size and surface area.[1] The Twin Polymerization (TP) presents such a novel concept, which provides organic-inorganic hybrid materials composed of a phenolic resin and silica with interpenetrating phase nanodomains of dimensions below 3 nm.[2] The concept of TP is based on a concerted formation of two polymers in one synthetic step starting from a molecular precursor,[3] which in addition to experimental work is supported by theoretical investigations.[4] The most prominent example is based on TP of 2,2'-spirobi[4*H*-1,3,2-benzodioxasiline] (Si-spiro) and gave, after oxidation, SiO_2 with a surface area of more than 900 m^2/g and, after carbonization and treatment with HF, porous carbon with a surface area of more than 1200 m^2/g.[4c, 5] Recently, extension of the TP approach provided two novel concepts, i) the Simultaneous Twin Polymerization (STP)[6] and ii) the Additive-based Twin Polymerization (AbTP).[7] For example, polymerization of Si-spiro in the presence of polymerizable precursors (STP) and tin containing additives (AbTP), respectively, gives access to homogeneously distributed tin nanoparticles in a porous carbon / silica matrix after treatment under reductive conditions using hydrogen.[7] We decided to explore, whether TP also offers the possibility to synthesize nanoparticular alloys starting from Si-spiro, the polymerizable tin(II)-2,4-dimethoxyphenylmethanolate (**1**) and metal carboxylates as additives. The STP of Si-spiro and tin(II) alkoxide **1** was expected to give interpenetrating organic-inorganic networks, in which the additional metal source is trapped during the polymerization process. It was envisaged that subsequent treatment (of the as-prepared materials) under reducing conditions provides nanoparticular tin alloys embedded in a carbon / silica matrix (Scheme 1).

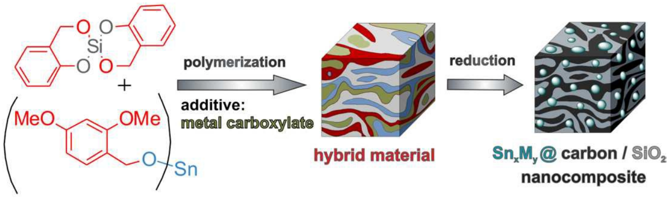

Scheme 1. General concept for the synthesis of nanoparticular tin alloys embedded in a carbon / silica matrix.

---

[a] Technische Universität Chemnitz, Fakultät für Naturwissenschaften, Institut für Chemie, Professur Koordinationschemie, D-09107 Chemnitz, Germany.
[b] Technische Universität Chemnitz, Fakultät für Naturwissenschaften, Institut für Chemie, Professur Polymerchemie, D-09107 Chemnitz, Germany.
[c] BASF SE, Carl-Bosch Straße 38, D-67056 Ludwigshafen, Germany.
* Corresponding author. Fax: +49 (0) 371 531 21219.
E-mail: michael.mehring@chemie.tu-chemnitz.de

†Electronic Supplementary Information (ESI) available: [details of any supplementary information available should be included here]. See DOI: 10.1039/x0xx00000x

As demonstrated previously, the resulting silica acts as a crystal growth inhibitor and prevents sintering of the tin nanoparticles during the treatment with hydrogen, which resulted in homogeneously distributed tin nanoparticles within a carbon / silica matrix.[7] The variation of type and concentration of the metal containing additives was anticipated to allow the selective synthesis of different tin alloys which are promising materials for a variety of applications such as bimetallic catalysts,[8] lead-free solder materials used for e.g. electrical devices in chip technology,[9] and especially as alternative anode materials for lithium-ion batteries.[10] Here we present experimental results on this novel synthetic strategy in the field of TP.

Results and discussion

Nanocomposite prepared by Simultaneous Twin Polymerization

The Simultaneous Twin Polymerization (STP) of 2,2'-spirobi[4*H*-1,3,2-benzodioxasiline] (Si-spiro) with a new tin(II) alkoxide, tin(II)-2,4-dimethoxyphenylmethanolate (**1**), in toluene was chosen as basic system for the synthesis of tin-containing organic-inorganic hybrid materials. Subsequent treatment under reductive conditions (Ar/H_2) reduces the amount of carbonous material and converts tin oxide into tin while maintaining the SiO_2 matrix. We have previously shown that this strategy allows the formation of tin nanoparticles within a carbon / silica matrix with homogeneous distribution.[7] The 2,4-dimethoxyphenylmethanolate was used as organic ligand for the tin(II)-precursor due to its ability to provide high solubility and increased reactivity in the TP reaction. In a typical approach Si-spiro is mixed with the tin(II) alkoxide **1** in toluene and provides a violet precipitate (hybrid material **2a**) after heating to 105 °C. The polymerization is initiated by the Lewis acidic nature of the tin(II)alkoxide, which is confirmed by Differential Scanning Calorimetry (DSC) (Figure 1).

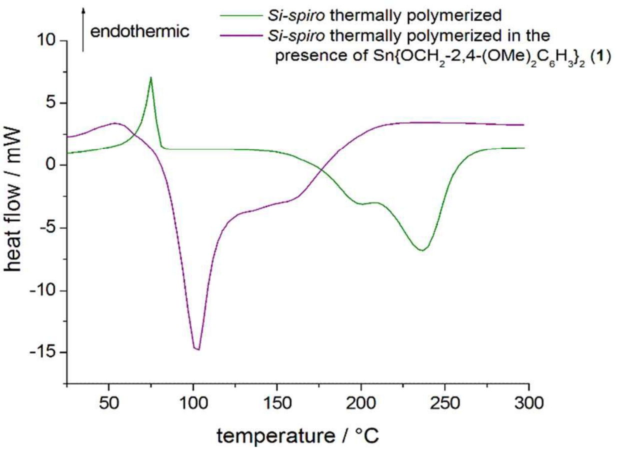

Figure 1. Differential scannig calorimetry (DSC) curve of Si-spiro thermally polymerized as compared to the polymerization of Si-spiro initiated by $Sn\{OCH_2\text{-}2,4\text{-}(OMe)_2C_6H_3\}_2$.

The DSC curve for Si-spiro shows an endothermic process around 80 °C, which is assigned to melting, and a broad exothermic process with an onset temperature of 169 °C. The exothermic process, is assigned to the formation of the phenolic resin and the subsequent condensation reaction to form the silica network.[2b, 4c] In comparison, the DSC curve of Si-spiro in the presence of the tin(II) alkoxide **1** indicates a broad endothermic process at 54 °C, immediately followed by an exothermic process with an onset temperature of 84 °C, which is indicative for an inititation of the TP by the Lewis acidic tin alkoxide. The exothermic process is also indicated by a broad signal, with an intense peak in the first part and a broad peak in the second part, which is indicative for two steps during the polymerization reaction. Solid-state ^{13}C NMR spectroscopy of the as-prepared hybrid material **2a** gave the expected signals, which are assigned to a phenolic resin with ortho/ortho' and ortho/para' substitution.[11] Additional signals at 55 and 95 ppm are assigned to the polymerized tin (II) alkoxide **1** (Figure 2). The solid-state ^{29}Si NMR spectrum shows a broad signal at $\delta \approx -100$ ppm which is in the range between signals expected for Q_2 and Q_4 moieties and thus indicative for incompletely condensed silica (Figure 2).

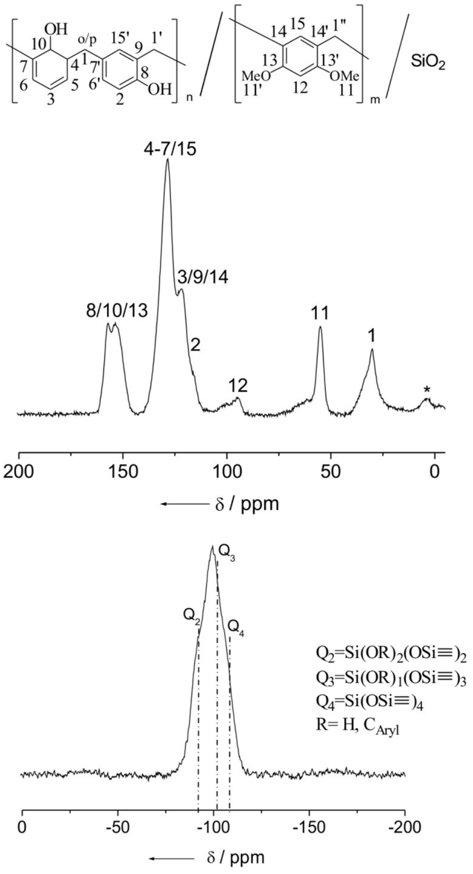

Figure 2. Solid state $^{13}C\{^1H\}$ CP MAS NMR spectrum and $^{29}Si\{^1H\}$ CP MAS NMR spectrum of hybrid material **2a**. Asterisks (*) indicate spinning side bands.

Notably, the comparison of the solid-state ^{13}C and ^{29}Si NMR spectra of **2a** with the hybrid material obtained from the TP of Si-spiro confirms the formation of a phenolic resin and a silica network (Figure S1, Figure S2).[5] Furthermore, HAADF-STEM analysis of the resulting phenolic resin/SiO_2 hybrid material (**2a**) shows the typical morphology of twin polymers with homogenously distributed nanodomains with sizes below 3 nm (Scheme 2).[3, 5] Subsequent treatment of the hybrid material **2a** under reductive conditions (600 °C; Ar/H_2, 95/5 %) gave homogeneously distributed tin nanoparticles in a carbon / silica matrix (**2a-r**) (Scheme 2).

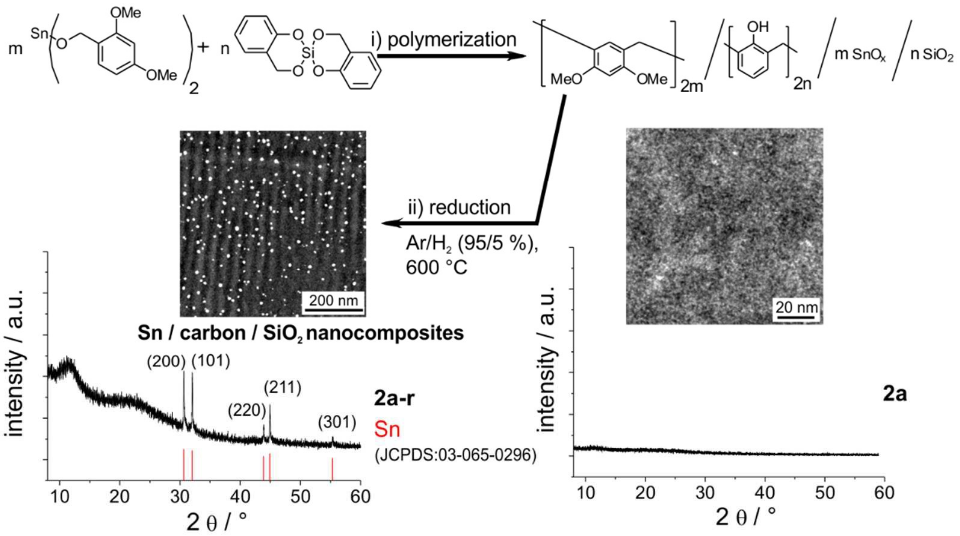

Scheme 2. i) Simultaneous Twin Polymerization (STP) of Si-spiro with tin(II)-2,4-dimethoxyphenylmethanolate (**1**) and ii) the reduction of hybrid material **2a**. PXRD pattern of hybrid material **2a** and HAADF-STEM image (right) compared with the PXRD pattern and HAADF-STEM image of the nanocomposite **2a-r** as obtained after the reduction process (left).

To investigate the influence of the Si/Sn-ratio on the resulting particle sizes and BET surface areas, we used an increased tin ratio for **2b** (1:1) compared to **2a** (3:1). Measurements of the Brunauer–Emmett–Teller (BET) surface area of the nanocomposites **2a-r** and **2b-r** revealed quite similar values of 313 m^2/g and 327 m^2/g, respectively (Table 1). Selected area electron diffraction (SAED) studies and powder X-ray diffraction (PXRD) analyses confirmed the formation of tin nanoparticles in both compounds (Figure S3). High-angle annular dark field scanning transmission electron microscopy (HAADF-STEM) reveals the formation of 5-20 nm (**2a-r**) and 10-40 nm (**2b-r**) sized tin particles within the carbon / silica matrix. In addition, a few isolated tin particles at the surface of the carbon/silica matrix with particle sizes in the range of 30-70 nm (**2a-r**) and 30-150 nm (**2b-r**) were observed (Figure 3, Figure S4). However, the average crystallite size of 35 nm (**2a-r**) and 27 nm (**2b-r**) as calculated by the Scherrer equation are in accordance with the observed particle sizes based on HAADF-STEM images of **2a-r** and **2b-r**. The increased tin content in **2b-r** provides a higher amount of tin particles embedded in the C/SiO_2-matrix which partially tend to agglomerate. Thus, the reduced SiO_2 content in **2b-r** leads to an incresaed sintering behavior during the reduction compared to **2a-r** and provides larger particles. In conclusion, the experimental results confirm the suitability of our approach for the synthesis of nanocomposites composed of tin nanoparticles in a matrix of carbon and silica.

Nanocomposites prepared by addition of metal containing additives

To probe the potential of our approach for the synthesis of nanoparticular tin alloys embedded in a carbon / silica matrix different amounts of metal containing additives were mixed with the basic system, Si-spiro and tin(II) 2,4-dimethoxyphenylmethanolate (**1**) (Scheme 3). Metal 2-[2-(2-methoxyethoxy)ethoxy]acetates and undecane-1-carboxylates were used due to their high solubility in toluene. In order to maintain phase-pure tin alloys such as Sn_2Co, Sn_2Fe, Sn_4Ni_3 and Sn_5Cu_6 appropriate M/Sn-ratios (M = metal additive) were used. TP provided the hybrid materials **2-6** (Table 1). All samples were polymerized in toluene at 105 °C and gave pale colored amorphous powders after work up.

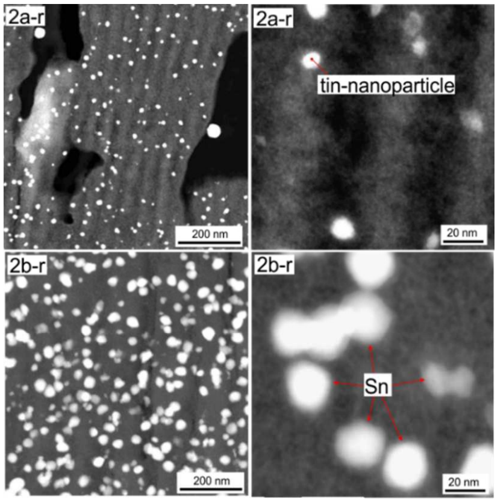

Figure 3. HAADF-STEM images of the nanocomposites (Sn/C/SiO_2) **2a-r** and **2b-r**. The black grooves result from the sample preparation.

Selected solid-state ^{13}C NMR spectra of the as-prepared hybrid materials gave signals, that are assigned to a phenolic resin with ortho/ortho' and ortho/para' substitution and additional signals in the range of 55-95 ppm, which are assigned to the polymerized tin (II) alkoxide **1** and the ethoxy-group of the metal containing additives as exemplarily is shown in Figure S5.

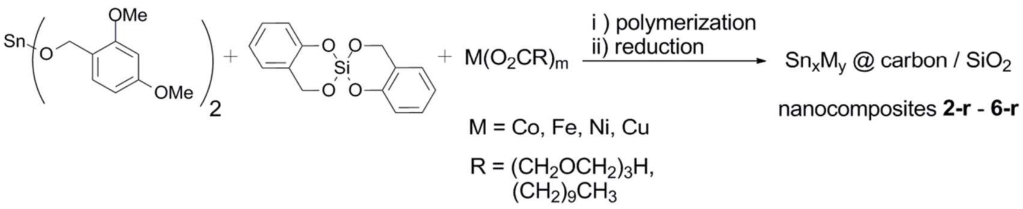

Scheme 3. STP of Si-spiro with tin(II)-2,4-dimethoxyphenylmethanolate (**1**) in the presence of metal containing additives gave after reduction (Ar/H_2, 95/5 %) the nanocomposites **2-r** – **6-r**.

Table 1. BET surface areas, particle sizes, tin and carbon contents of the reduced hybrid materials **2-r** – **6-r**.

reduced hybrid materials (ratio Sn:Si in mol %)	**metal additive (ratio Sn:M in mol %)**	**BET surface area in m^2/g**	**average particle size in nm[a]**	**tin content in wt.%[b]**	**carbon content in wt.%[c]**
2a-r (3:1)	-	313	35	29	47
2b-r (1:1)	-	327	27	n.d.	46
3a-r (3:1)	$Co(O_2CR^1)_2$ (1:0.1)	324	21	24	47
3b-r (1:1)	$Co(O_2CR^1)_2$ (1:0.22)	244	32.	35	41
3c-r (3:1)	$Co(O_2CR^1)_2$ (1:0.33)	321	28	n.d.	44
4a-r (3:1)	$Fe(O_2CR^1)_3$ (1:0.3)	209	45	17	43
4b-r (3:1)	$Fe(O_2CR^1)_3$ (1:0.5)	251	81	n.d.	49
5a-r (3:1)	$Ni(O_2CR^1)_2$ (1:0.75)	123	n.d.	14	42
5b-r (1:1)	$Ni(O_2CR^1)_2$ (1:0.3)	< 10	n.d.	37	38
6-r (3:1)	$Cu(O_2CR^2)_2$ (1:1.2)	231	33	16	48

[a] calculated by the Scherrer equation. [b] measured with x-ray fluorescence analysis. [c] measured by C,H analysis. n.d. = not determined. $R^1=(CH_2OCH_2)_3H$; $R^2=(CH_2)_9CH_3$.

Noteworthy, in the solid-state ^{29}Si NMR (for hybrid material **5a**) a signal around $\delta = -103$ ppm was assigned, which indicates a higher content of Q_4 moieties and consequently an increased degree of cross-linking in the silica network as compared to the hybrid material **2a** (Figure S6). However, the intensity of the signal for hybrid material **5a** as compared to hybrid material **2a** is quite low, which can be explained by the paramagnetic influence of the additives. It should be noted that for **3b** the solid-state ^{29}Si NMR signal is completely lacking as a result of the latter influence.[12] Finally, the hybrid materials **2-6** were treated under reducing conditions (600 °C 780 °C, Ar/H_2, 95/5 %) to give black solid nanocomposites. Table 1 provides information on the metal containing additives used together with the tin(II) alkoxide (**1**), corresponding BET surface areas, particle sizes and tin contents of the resulting reduced hybrid materials **2-r** – **6-r**. In a typical experiment cobalt(II)-2-[2-(2-methoxyethoxy)ethoxy]acetate was mixed in different amounts with the silicon and tin precursors (Si/Sn/Co-ratio: 3:1:0.1 for **3a-r**, 1:1:0.22 for **3b-r** and 3:1:0.33 for **3c-r**) to probe the influence on surface area and particle size of the nanocomposites and the possibility to form the alloy Sn_2Co within the matrix. The powder X-ray diffraction and selected-area electron diffraction of the resulting nanocomposites **3a-r** and **3b-r** confirmed the formation of the Sn_2Co alloy, but in addition elemental tin was also detected (Figure S7). We attribute this to the high tin content used in both composites (Sn/Co-ratio: 1:0.1 for **3a-r** and 1:0.22 for **3b-r**) and the high temperature during the reduction process of 600 °C, which is well above the melting point of tin. Thus leaching of tin to the surface of the material is promoted. The application of temperatures below 600 °C gave amorphous composites. A further increase of the cobalt ratio in **3c-r** (Sn/Co-ratio: 1:0.33) gave, in addition to the expected Sn_2Co alloy, also minor parts of the SnCo alloy as shown by PXRD and SAED analysis (Figure S8). A Sn/Co-ratio of 1:0.5 lead to the formation a pure SnCo alloy (Figure S9). Therefore, we used the adapted tin/metal additive-ratio to produce the tin alloys. BET surface areas of the reduced nanocomposites amount to 324 m^2/g for **3a-r**, 244 m^2/g (24 wt.% tin) for **3b-r** (35 wt.% tin) and 321 m^2/g for **3c-r**. Notably, the higher cobalt content as used in **3b-r** (Si/Sn/Co-ratio: 1:1:0.22) as compared to **3a-r** results in an increased amount of Sn_2Co alloy in the final nanocomposites, whereas a higher tin content (35 wt.%) results in larger particle sizes (**3b-r**: 32 nm, **3a-r**: 21 nm) as calculated on the basis of PXRD (Figure S7). The HAADF-STEM images are in accordance with the calculated average particle sizes and show homogeneously distributed Sn_2Co particles with sizes of 6-20 nm (**3a-r** and **3c-r**) and 10-80 nm (**3b-r**), respectively, within the carbon / silica matrix (Figure 4, Figure S10). In addition, a few isolated tin particles at the surface of the carbon

/ silica matrix with particles sizes of 20-80 nm (**3a-r** and **3c-r**) and partially agglomerated particles with sizes up to 500 nm (**3b-r**) were also observed (Figure 4, Figure S11). Hence, the higher cobalt content in **3c-r** provides similar particle sizes and surface areas as compared to **3a-r**, whereas the reduced SiO_2 content in **3b-r** leads to larger particles due to increased sintering during the reduction. Another additive, that was mixed in different amounts with the basic system, is iron(III) undecanate (Si/Sn/Fe-ratio: 3:1:0.3 for **4a-r** and 3:1:0.5 for **4b-r**). After the reduction process, nanocomposites with BET surface areas of 209 m^2/g (**4a-r**) and 251 m^2/g (**4b-r**), respectively, were observed. Analysis by HAADF-STEM reveals homogeneously distributed particles inside the C/SiO_2 matrix with particle sizes in the range of 20-60 nm for **4a-r** and larger particles with sizes in the range of 20-140 nm for **4b-r** (Figure 5). However, selected area electron diffraction (SAED) of both nanocomposites reveals that in addition to Sn_2Fe particles tin is also detected.

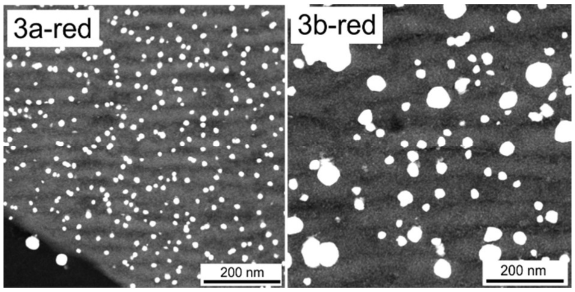

Figure 4. HAADF-STEM images of the nanocomposites $Sn_2Co/C/SiO_2$ **3a-r** and **3b-r**.

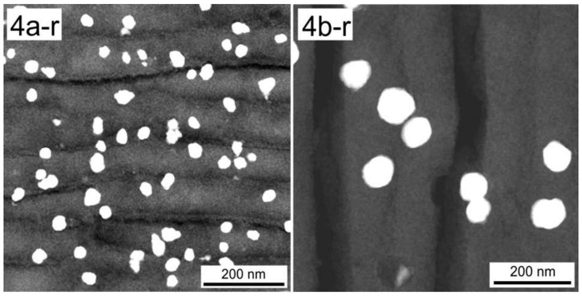

Figure 5. HAADF-STEM images of the nanocomposites $Sn_2Fe/C/SiO_2$ **4a-r** and **4b-r**. The black grooves in the right image are attributed to sample preparation.

The use of a higher amount of iron reduces the amount of tin, but elemental Sn is still present in the final material. The PXRD analyses confirm these results. Particle sizes of 45 nm (**4a-r**) and 81 nm (**4b-r**) are calculated from PXRD, and tin is detected in addition to Sn_2Fe (Figure S12). In order to synthesize Sn_4Ni_3 within the carbon / silica matrix a Si/Sn/Ni-ratio of 3:1:0.75 was used. Energy dispersive X-ray spectroscopy of the as-prepared nanocomposite **5a-r** reveals a Ni/Sn-ratio of about 0.67. PXRD analysis gave broad reflexes which do not allow to distinguish between Sn_4Ni_3 and Sn_2Ni_3, but SAED is in favour of formation of Sn_2Ni_3 (Figure S13). The HAADF-STEM images show homogenously distributed Sn/Ni-nanoparticles within the carbon / silica matrix with a quite narrow particle size distribution of 3-10 nm and only minor contents of Sn/Ni-particles located outside the matrix (Figure 6, Figure S14).

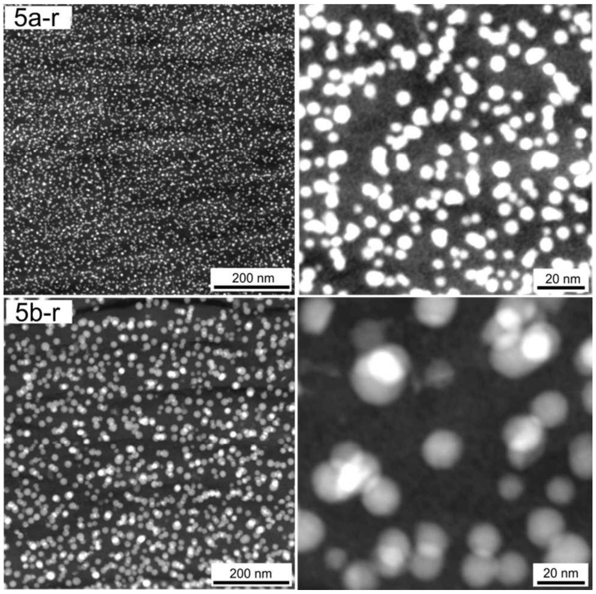

Figure 6. HAADF-STEM images of the nanocomposites $Sn_2Ni_3/C/SiO_2$ (**5a-r**) and $Sn_4Ni_3/C/SiO_2$ (**5b-r**).

Using a higher content of tin (Si/Sn/Ni-ratio of 1:1:0.3) provides a material for which PXRD is again not unambiguously regarding formation of the tin-alloy, but indicates formation of tin as an additional phase. Selected area electron diffraction indicates formation of Sn_4Ni_3 and Sn (**5b-r**) (Figure S15). The increased tin content of 35 wt.% (**5b-r**) compared to 14 wt.% (**5a-r**) results in larger particle sizes of 10-22 nm within the carbon / silica matrix (Figure 6). BET analysis of the nanocomposites **5a-r** and **5b-r** show quite low surface areas of 123 m^2/g and < 10 m^2/g, respectively. The material **5a-r** ($Sn_2Ni_3/C/SiO_2$ nanocomposite) was chosen to test the potential of the here described nanocomposites as anode materials for lithium-ion batteries. Nanocomposite **5a-r** shows the smallest particles (3-10 nm) within the C/SiO_2 matrix and a negligible content of Sn/Ni-aggregates outside the matrix. It shows an initial discharge capacity (delithiation) of around 910 mAh g^{-1} due to the surface reactions with the electrolyte and the formation of a stable SEI (solid electrolyte interface) layer during the first cycle.[13] After activation in the initial cycle, the anode was cycled at current density of 30 mAg^{-1}, exhibiting capacities of 510 and 386 $mAhg^{-1}$ for the 2th and 17th cycles, respectively (Figure S16). The nanocomposite **5a-r** retains after 17th cycles a capacity of around 76 %. These preliminary results demonstrate the potential of the approach for the development of anode materials for lithium-ion batteries. Finally, a copper carboxylate was used as additive for the basic system. A Si/Sn/Cu-ratio of 3:1:1.2 produced the nanocomposite **6**, but an additional amount of $SnCl_4$ (10 mol %) was necessary to initiate the polymerization. The PXRD analysis and selected area electron diffraction of the final nanocomposite **6-r** reveals the formation of a pure phase domain of a tin alloy of the composition Sn_5Cu_6 (Figure 7, Figure S17), a BET surface area of 231 m^2/g and a tin content of 16 wt. %.

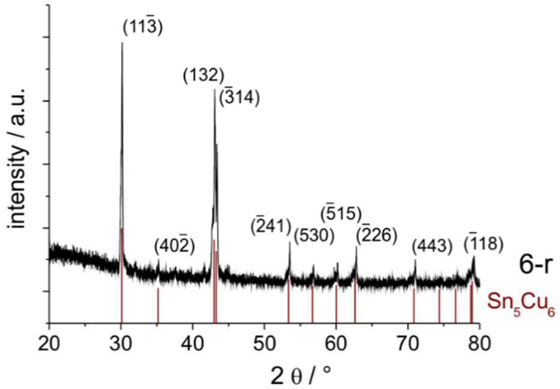

Figure 7. Powder X-ray diffraction (PXRD) pattern of the nanocomposite **6-r** (Ar/H_2, 95/5 %; heating rate: 5 K min^{-1}, final temperature: 600 °C, time 2 h); (Sn_5Cu_6: JCPDS 01-072-8761).

PXRD analysis reveals an average particle size of 33 nm, calculated by use of the Scherer equation. HAADF-STEM images show a large particle size distribution of 25-350 nm and compared to the nanocomposites **2-r** - **5-r** a less densely packed carbon / silica matrix which might be attributed to the addition of $SnCl_4$ in the first step (Figure 8). As a result of this less densely packed carbon / silica matrix an increased agglomeration of the Sn_5Cu_6 particles occurs during the reduction process producing particles of larger size in the final material.

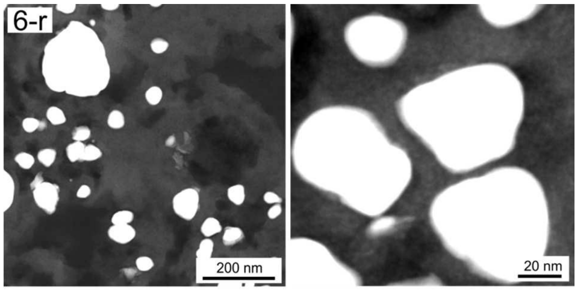

Figure 8. HAADF-STEM images of the nanocomposite $Sn_5Cu_6/C/SiO_2$ **6-r**.

Conclusions

A new tin(II) alkoxide, tin(II)-2,4-dimethoxyphenylmethanolate, was synthesized and polymerized together with 2,2'-spirobi[*4H*-1,3,2-benzodioxasiline] (Si-spiro) in the presence of different metal containing additives, following the approach of Additive-based Simultaneous Twin Polymerization (AbSTP). The resulting hybrid materials are composed of SiO_2, metal-containing species and a phenolic resin and gave, after treatment under reductive conditions (600 °C-780 °C, Ar/H_2, 95/5 %), a variety of tin alloys (Sn_2Co, Sn_2Fe, Sn_2Ni_3, Sn_4Ni_3, and Sn_5Cu_6) embedded in a carbon / silica matrix with particle sizes in the nanometer range and with homogeneous distribution. BET-analyses of the final composites exhibit surface areas in the range of 10 - 327 m^2/g, where low amounts of additives correlate with the higher values. Variation of the ratio Sn/Ni allows for the formation of either Sn_2Ni_3 or Sn_4Ni_3 in the final nanocomposites **5a-r** and **5b-r**. The smallest particles with a narrow size distribution of 3-10 nm were observed for the nanocomposite composed of Sn_2Ni_3 within the carbon / silica matrix (**5a-r**). In most cases we detected residual amounts of tin in the nanocomposites, but a pure alloy was observed for the composite $Sn_5Cu_6/C/SiO_2$ (**6-r**). As we have reported previously for tin-containing nanocomposites, the silica prevents sintering of the nanoparticles during the reduction process, but it does not hamper the formation of alloys within the carbon / silica matrix. This novel approach might offer access to diverse porous alloy/C/SiO_2 nanocomposites e.g., for the development of novel nanocomposites as anode materials for lithium ion batteries, exemplarily demonstrated for Sn_2Ni_3.

Experimental

Starting materials and instrumentation

All reactions were carried out under argon atmosphere with use of the Schlenk technique. Diethyl ether, *n*-hexane, *n*-butanol and toluene were dried over sodium and freshly distilled prior use. The starting materials tin(II)methoxide, 2,2'-spirobi[*4H*-1,3,2-benzodioxasiline], cobalt(II)-2-[2-(2-methoxyethoxy)ethoxy]acetate, nickel(II)-2-[2-(2-methoxyethoxy)ethoxy]acetate, iron(III) undecanate and copper(II) undecanate were prepared by modified literature procedures.[5, 14]

^1H, $^{13}C\{^1H\}$, and $^{119}Sn\{^1H\}$ NMR data were recorded on a Bruker Avance III 500 spectrometer at 500.3, 125.8, and 186.4 MHz, respectively. The spectra were referenced to $SiMe_4$ (δ = 0 ppm for ^1H, ^{13}C) and $SnMe_4$ (δ = 0 ppm for ^{119}Sn). Solid-state NMR measurements were performed at 9.4 T on a Bruker Avance 400 spectrometer equipped with double-tuned probes capable of magic angle spinning (MAS). $^{13}C\{^1H\}$ CP MAS NMR spectroscopy was accomplished in 4 mm rotors made of zirconium oxide spinning at 12.5 kHz. Cross-polarization with contact times of 3 ms was used to enhance sensitivity. The recycle delay was 5 s. $^{119}Sn\{^1H\}$ CP MAS NMR spectroscopy was performed in 4 mm rotors spinning at 12.5

kHz. The recycle delay was 10 s. All spectra were obtained under ^{1}H decoupling using a two-pulse phase modulation sequence. The spectra were referenced with respect to tetramethylsilane (TMS) using tetracyclohexylstannane as a secondary standard (δ = 3.6 ppm for ^{13}C, δ = -97.3 ppm for ^{119}Sn). If not stated otherwise, all spectra were acquired at room temperature. Powder X-ray diffraction (PXRD) patterns were measured with a STOE-STADI-P diffractometer using CuKα radiation (40 kV, 40 mA). The crystallite size was estimated by using the formula determined by the Scherrer equation: $\tau = K\lambda/\beta\cos\theta$, in which τ is the volume weighted crystallite size in nm, K is the Scherrer constant here taken as 1.0, λ is the X-ray wavelength, ⍰ is the Bragg angle in rad, and β is the full width of the diffraction line at half of the maximum intensity. For X-ray fluorescence analysis a MiniPal PW 4025/00 X-ray spectrometer with a rhodium anode (type TFS 5109/ Rh) at 15 kV and 0.040 mA was used (regression factor = 1.6 %). Elemental analysis was performed by a Thermo Type Flash AE 1112 elemental analyzer. Specific surface area analyses were performed with N_2 adsorption–desorption isotherms at liquid nitrogen temperature (77 K) using a Quantachrome Autosorb IQ2 apparatus, and were evaluated by the Brunauer–Emmett–Teller (BET) method at the p/p_0 ratio of 0.150. The high-angle annular dark-field (HAADF)–scanning electron transmission microscopy (STEM) was performed by using a FEI Tecnai F20 field-emission transmission electron microscope. The samples (embedded in an epoxy resin) were cut ultrathin by a Leica UCT ultramicrotome. The ultrathin slices were transferred onto a carbon-coated copper perforated grid.

Synthesis of tin(II)-2,4-dimethoxyphenylmethanolate (1):

2,4-dimethoxybenzyl alcohol (3.91 g, 23.25 mmol) in 10 ml toluene was added dropwise to a stirred suspension of tin(II)methoxide (2.00 g, 11.06 mmol) in 60 ml toluene. After stirring for 1 h at room temperature the resulting methanol was removed and the suspension changed to a clear solution. The remaining solvent was then evaporated and the residue was washed several times with diethyl ether (15 ml) and dried under vacuum (10^{-3} mbar). Yield 3.98 g (8.78 mmol, 79 %) of a colorless solid.

Decomposition at 160 °C; ^{1}H NMR (500.30 MHz, $CDCl_3$): δ = 3.75 (s, 3 H, 4-MeO), 3.80 (s, 3 H, 2-MeO), 4.76 (s, 2 H, CH_2), 6.40 (dd, 2 H, H^5, H^6), 7.20 ppm (s, 1 H, H^3); ^{13}C{^{1}H} NMR (125.81 MHz, $CDCl_3$) $\delta =$ 55.3, 54.9 (MeO), 60.6 (CH_2), 98.3 (C^3), 103.8 (C^5), 124.6 (C^1), 130.1 (C^6), 158.2 (C^2), 160.3 ppm (C^4); ^{119}Sn{^{1}H} NMR (186.53 MHz, C_6D_6) δ = -158 ppm; ^{119}Sn{^{1}H} CP MAS NMR (149.17 MHz) δ = - 350 ppm; IR: $\nu =$ 2936 (w), 2838 (w) 1590 (s), 1501 (s), 1457 (s), 1370 (m), 1285 (s), 1254 (m), 1204 (s), 1156 (s), 1123 (s) (C-O ν), 1032 (s), 986 (s), 932 (m), 822 (s), 731 (s), 695 (m), 627 (m), 571 (s), 517 (m), 455 cm^{-1} (s); elemental analysis calcd (%) for $C_{18}H_{22}O_6Sn$ (453.07): C 47.7, H 4.9; found: C 47.4, H 4.6.

Synthesis of hybrid materials (Gerneral method)

The hybrid materials were prepared according the general synthetic approach as follows:

In a typical reaction 2,2'-spirobi[*4H*-1,3,2-benzodioxasiline] and tin(II)-2,4-dimethoxyphenylmethanolate (**1**) were suspended in toluene and heated to 90 °C. The colorless solution changed to a red color and the metal containing additive was added. The reaction mixture was then heated to 105 °C and after stirring for 12 hours the as obtained precipitate was filtered off, washed three times with acetone (10 ml) and dried in vacuo. Further experimental details are collected in the Supporting Information.

Reduction process (Gerneral method)

All reduction processes of the hybrid materials were performed in a tube furnace with a heating rate of 5 K min^{-1}, a reaction time of 2 h in total and a final reaction temperature of 600 °C for materials **2-r** – **4-r**, **6-r** and 3 h at 780 °C for materials **5a-r** and **5b-r**. The solids were treated constantly with an Ar/H_2 (95/5 %) stream of flow rate 30 L h^{-1} to give black solids (57-70 wt.%) composed of nanostructured tin alloys embedded in a C/SiO_2 matrix.

Acknowledgements

We thank Prof. Dr. S. Spange for access to differential scanning calorimetry and X-ray fluorescence spectroscopy. The Authors would also like to thank Dr. H. Wolf and Dr. C. Erk for performing electrochemical measurements. We are grateful to the BASF Aktiengesellschaft Ludwigshafen and the Deutsche Forschungsgemeinschaft (FOR 1497 ”organic–inorganic nanocomposites through twin polymerization“) for financial support.

References

[1] a) G. Kickelbick, *Hybrid Materials-Synthesis Characterization, and Applications*, Wiley-VCH, Weinheim, **2007**; b) C. Sanchez, P. Belleville, M. Popall, L. Nicole, *Chem. Soc. Rev.* **2011**, *40*, 696; c) L. Nicole, C. Laberty-Robert, L. Rozes, C. Sanchez, *Nanoscale* **2014**, *6*, 6267; d) C. Sanchez, C. Boissiere, S. Cassaignon, C. Chaneac, O. Durupthy, M. Faustini, D. Grosso, C. Laberty-Robert, L. Nicole, D. Portehault, F. Ribot, L. Rozes, C. Sassoye, *Chem. Mater.* **2014**, *26*, 221.

[2] a) S. Grund, P. Kempe, G. Baumann, A. Seifert, S. Spange, *Angew. Chem. Int. Ed.* **2007**, *46*, 628; b) P. Kempe, T. Löschner, A. A. Auer, A. Seifert, G. Cox, S. Spange, *Chem. Eur. J.* **2014**, *20*, 8040; c) C. Schliebe, T. Gemming, L. Mertens, M. Mehring, H. Lang, *Eur. J. Inorg. Chem.* **2014**, *2014*, 3161; d) F. Böttger-Hiller, R. Lungwitz, A. Seifert, M. Hietschold, M. Schlesinger, M. Mehring, S. Spange, *Angew. Chem. Int. Ed.* **2009**, *48*, 8878; e) C. Schliebe, T.

Gemming, J. Noll, L. Mertens, M. Mehring, A. Seifert, S. Spange, H. Lang, *ChemPlusChem* **2015**, *80*, 559.

[3] T. Ebert, A. Seifert, S. Spange, *Macromol. Rapid Commun.* **2015**.

[4] a) A. A. Auer, A. Richter, A. V. Berezkin, D. V. Guseva, S. Spange, *Macromol. Theor. Simul.* **2012**, *21*, 615; b) T. Schönfelder, J. Friedrich, J. Prehl, S. Seeger, S. Spange, K. H. Hoffmann, *Chem. Phys.* **2014**, *440*, 119; c) P. Kitschke, A. A. Auer, T. Löschner, A. Seifert, S. Spange, T. Rüffer, H. Lang, M. Mehring, *ChemPlusChem* **2014**, *79*, 1009; d) I. Tchernook, J. Prehl, J. Friedrich, *Polymer* **2015**, *60*, 241.

[5] S. Spange, P. Kempe, A. Seifert, A. A. Auer, P. Ecorchard, H. Lang, M. Falke, M. Hietschold, A. Pohlers, W. Hoyer, G. Cox, E. Kockrick, S. Kaskel, *Angew. Chem. Int. Ed.* **2009**, *48*, 8254.

[6] T. Löschner, A. Mehner, S. Grund, A. Seifert, A. Pohlers, A. Lange, G. Cox, H.-J. Hähnle, S. Spange, *Angew. Chem. Int. Ed.* **2012**, *51*, 3258.

[7] C. Leonhardt, S. Brumm, A. Seifert, A. Lange, S. Csihony, M. Mehring, *ChemPlusChem* **2014**, *79*, 1440.

[8] a) V. S. Antonin, M. H. M. T. Assumpcao, J. C. M. Silva, L. S. Parreira, M. R. V. Lanza, M. C. Santos, *Electrochim. Acta* **2013**, *109*, 245; b) A. Onda, T. Komatsu, T. Yashima, *J. Catal.* **2001**, *201*, 13; c) F. Xie, X. Chu, H. Hu, M. Qiao, S. Yan, Y. Zhu, H. He, K. Fan, H. Li, B. Zong, X. Zhang, *J. Catal.* **2006**, *241*, 211.

[9] a) L. Liu, C. Andersson, J. Liu, *J. Electron. Mater.* **2004**, *33*, 935; b) S.-W. Chen, Y.-K. Chen, H.-J. Wu, Y.-C. Huang, C.-M. Chen, *J. Electron. Mater.* **2010**, *39*, 2418; c) P. Sun, C. Andersson, X. Wei, Z. Cheng, D. Shangguan, J. Liu, *Mater. Sci. Eng. B* **2006**, *135*, 134.

[10] a) P. P. Ferguson, M. L. Martine, A. E. George, J. R. Dahn, *J. Power Sources* **2009**, *194*, 794; b) B. Liu, A. Abouimrane, Y. Ren, M. Balasubramanian, D. Wang, Z. Z. Fang, K. Amine, *Chem. Mater.* **2012**, *24*, 4653; c) M. Chamas, P.-E. Lippens, J.-C. Jumas, K. Boukerma, R. Dedryvère, D. Gonbeau, J. Hassoun, S. Panero, B. Scrosati, *J. Power Sources* **2011**, *196*, 7011; d) Z. Edfouf, F. Cuevas, M. Latroche, C. Georges, C. Jordy, T. Hézèque, G. Caillon, J. C. Jumas, M. T. Sougrati, *J. Power Sources* **2011**, *196*, 4762; e) J. Hassoun, G. A. Elia, S. Panero, B. Scrosati, *J. Power Sources* **2011**, *196*, 7767; f) F. Wang, M. Zhao, X. Song, *J. Alloy. Compd.* **2007**, *439*, 249; g) Y.-L. Kim, H.-Y. Lee, S.-W. Jang, S.-J. Lee, H.-K. Baik, Y.-S. Yoon, Y.-S. Park, S.-M. Lee, *Solid State Ionics* **2003**, *160*, 235.

[11] R. L. Bryson, G. R. Hatfield, T. A. Early, A. R. Palmer, G. E. Maciel, *Macromolecules* **1983**, *16*, 1669.

[12] a) V. I. Bakhmutov, B. G. Shpeizer, A. Clearfield, *Magn. Reson. Chem.* **2006**, *44*, 861; b) G. Mali, A. Ristic, V. Kaucic, *J. Phys.Chem. B* **2005**, *109*, 10711.

[13] a) E. Peled, *J. Electrochem. Soc.* **1979**, *126*, 2047; b) M. Winter, J. O. Besenhard, M. E. Spahr, P. Novák, *Adv. Mater.* **1998**, *10*, 725.

[14] a) R. Gsell, M. Zeldin, *J. Inorg. Nucl. Chem.* **1975**, *37*, 1133; b) S. C. Warren, M. R. Perkins, U. Werner-Zwanziger, J. W. Zwanziger, F. J. DiSalvo, U. Wiesner, *Z. Phys. Chem.* **2012**, *226*, 1219; c) D. Adner, M. Korb, S. Schulze, M. Hietschold, H. Lang, *Chem. Commun.* **2013**, *49*, 6855; d) D. Adner, S. Mockel, M. Korb, R. Buschbeck, T. Ruffer, S. Schulze, L. Mertens, M. Hietschold, M. Mehring, H. Lang, *Dalton Trans.* **2013**, *42*, 15599; e) Z. Yang, J. Shen, L. A. Archer, *J. Mater. Chem.* **2011**, *21*, 11092.

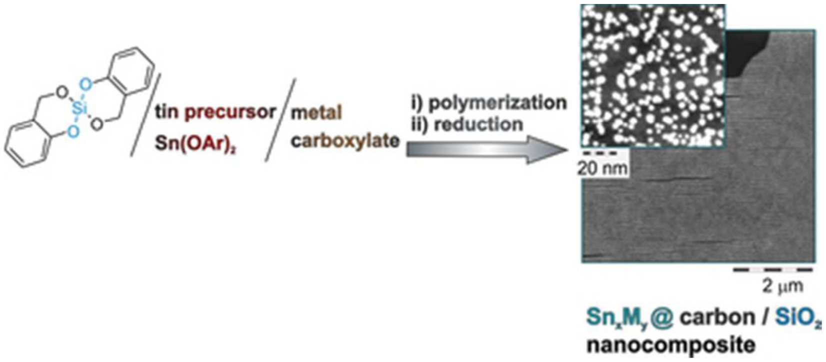

34x14mm (300 x 300 DPI)